Astron. Astrophys. 311, 858–872 (1996)

ASTRONOMY AND ASTROPHYSICS

Evolution of outflow activity around low-mass embedded young stellar objects

S. Bontemps[1], P. André[1], S. Terebey[2], and S. Cabrit[3,4]

[1] CEA/DSM/DAPNIA, Service d'Astrophysique, C.E. Saclay, F-91191 Gif-sur-Yvette Cedex, France
[2] IPAC 100-22, Caltech, Pasadena, CA 91125, USA
[3] Observatoire de Grenoble, BP 53, F-38041 Grenoble Cedex, France
[4] DEMIRM, Observatoire de Paris, 61 Av. de l'Observatoire, F-75014 Paris, France

Received 9 August 1995 / Accepted 4 January 1996

Abstract. We present a detailed study of outflow activity in a sample of 45 low-luminosity embedded young stellar objects (YSOs). We use maps in the J=2–1 line of ^{12}CO to characterize this activity for YSOs that are still sufficiently embedded to show molecular outflows. Our CO outflow survey benefits from coordinated millimeter continuum measurements of circumstellar masses which allow us to estimate the evolutionary states of the central driving sources. Our sample comprises 36 near-IR (Class I) protostars and 9 far-IR/submm (Class 0) protostars, and should be representative of the "self-embedded" phase of (low-mass) protostellar evolution characterizing young stars still surrounded by significant circumstellar envelopes. We find that virtually all the objects in our sample have detectable CO outflow activity. We make homogeneous estimates of the outflow momentum flux deposited in the close environment of the driving sources in order to assess the dynamical properties of the underlying driving winds/jets. As is well-known, a tight correlation between outflow energetics and driving source luminosity is found for Class I sources. However, Class 0 sources lie a factor of $\sim$ 10 above this correlation, suggesting they have qualitatively different (e.g., more powerful) CO outflows. In addition, we find that the outflow momentum flux correlates well with the circumstellar envelope mass of the exciting source for *both* Class I and Class 0 sources. We show that this new correlation is independent of the F_{CO}–L_{bol} correlation and most likely results from a more or less continuous decrease of outflow power with time during the accretion phase. For a young star of final mass $\sim$ 0.6 $M_\odot$, the outflow momentum flux is typically $F_{CO} \sim 10^{-4}\,M_\odot$km s^{-1}yr^{-1} at the early Class 0 stage and $F_{CO} \sim 2 \times 10^{-6}\,M_\odot$km s^{-1}yr^{-1} at the late Class I stage. We suggest that this decrease of outflow energetics reflects a corresponding decay in the mass accretion/infall rate.

Key words: stars: formation – ISM: jets and outflows – radio lines: ISM – stars: pre-main sequence – radio lines: stars

Send offprint requests to: bonte@ariane.saclay.cea.fr

1. Introduction

The prevalence of CO outflows around embedded young stellar objects (YSOs) has long been taken as evidence that mass loss is a necessary ingredient of the star formation process (e.g., Shu et al. 1987, and references therein). Indeed, outflows may provide a means to carry off the excess angular momentum of the accreting matter (e.g., Blandford & Payne 1982, Pudritz & Norman 1986, Lada & Shu 1990). Our understanding of the structure of molecular outflows has made significant progress recently: a growing body of observational and theoretical evidence indicates that the detected CO outflows represent ambient gas that has been progressively entrained by an underlying jet directly originating in the central star and/or its circumstellar disk/envelope (e.g., Stahler 1993, Raga & Cabrit 1993, Masson 1994). However, the detailed physics of the jet driving mechanism, the outflow "history" of a given YSO, and the exact role of the circumstellar environment are still poorly understood. The goal of the present study is to investigate possible evolutionary trends in the outflow activity of low-mass YSOs.

Various empirical stages of YSO evolution can be distinguished in the path leading from cloud core to (low-mass) main sequence star. The youngest observed YSOs are the Class 0 sources recently identified by André, Ward-Thompson, & Barsony (1993, hereafter AWB; see also André 1995 for a review), which are distinguished by unusually strong submillimeter continuum emission compared with their bolometric luminosity. These Class 0 YSOs, defined by $L_{submm}/L_{bol} > 5 \times 10^{-3}$ (where L_{submm} is the submillimeter luminosity measured longward of 350 μm), are best interpreted as very young protostars whose dense circumstellar envelope/cocoon still contains more mass than the central hydrostatic protostellar core. The next, still deeply embedded, YSO stage corresponds to the Class I sources of Lada (1987), which are detected in the near-infrared ($\lambda \sim 2$ μm) and have only moderate submillimeter continuum emission (e.g., André & Montmerle 1994; hereafter AM). They are interpreted as more evolved protostars surrounded by

both a disk and a residual circumstellar envelope of substellar mass ($\sim 0.1 - 0.3$ $M_\odot$ at most in ρ Ophiuchi; cf. AM). Finally, the most evolved YSO stages correspond to pre-main sequence stars (e.g., T Tauri stars) surrounded by a circumstellar disk, either optically thick (Class II) or optically thin (Class III) at $\lambda \lesssim 10$ μm, that no longer have a dense circumstellar envelope.

Millimeter continuum maps of optically thin dust emission may be used to make quantitative estimates of the circumstellar masses surrounding YSOs of all types, and are therefore a useful tool to track their evolution (e.g., AM). AWB proposed an age ordering of embedded YSOs based on the ratio L_{submm}/L_{bol} of submillimeter to bolometric luminosity. They suggested that, to first order, and in a statistical sense at least, this luminosity ratio should track the ratio $M_{env}/M_\star$ of envelope to stellar mass and thus decrease with protostellar age. In this paper we explore the relationship of outflows with protostellar properties, and we therefore adopt L_{submm}/L_{bol} as a practical, quantitative indicator of YSO evolution.

Our ideas concerning the time of onset of the outflow phenomenon have changed in recent years. Although it seems plausible that there should exist a "pure-infall" phase prior to the ignition of the outflow, the length of this phase is only loosely constrained by the observed statistics of CO outflows among Class I sources (e.g., Terebey et al. 1989, Parker et al. 1991). In fact, sources of well-developed outflows are surrounded by larger amounts of circumstellar material than "non-outflow" embedded sources on average (Cabrit & André 1991), suggesting they are younger. It is now known that the fastest and most collimated ("jet-like") CO outflows are detected around the youngest (Class 0) objects (e.g., Bachiller et al. 1990, André et al. 1990; see Bachiller & Gómez-González 1992 for a review). This shows that vigorous outflows occur very early on when the protostar has attained a small fraction of its final mass, and that the pure-infall phase is extremely short or even non-existent.

In order to study outflow activity as a function of YSO evolutionary state in a more systematic and quantitative way, we have conducted a homogeneous ^{12}CO(2–1) survey of the close environment of a broad sample of nearby, low-luminosity embedded YSOs. A homogeneous survey was deemed necessary in order to compute consistent outflow properties, and therefore avoid the large scatter otherwise introduced by using published data based on different outflow analysis techniques and telescopes (Cabrit and Bertout 1990). This CO survey also benefits from the results of coordinated millimeter continuum observations of the same YSOs which provide information on the mass and spatial distribution of their circumstellar material (e.g., AM; André, Cabrit et al., in prep.).

The layout of the paper is as follows. In Sect. 2, we give our source selection criteria (Sect. 2.1) and explain observational details (Sect. 2.2). Sect. 3 gives the results of our CO outflow survey (Sect. 3.1) and presents estimates for the outflow momentum fluxes (Sect. 3.2). In Sect. 4, we discuss our survey results from a statistical point of view (Sect. 4.1), we show that the strength of CO outflows tends to decrease in the course of YSO evolution (Sect. 4.2), and we suggest possible interpretations and implications for our understanding of low-mass star formation (Sect. 4.3). Our conclusions are summarized in Sect. 5.

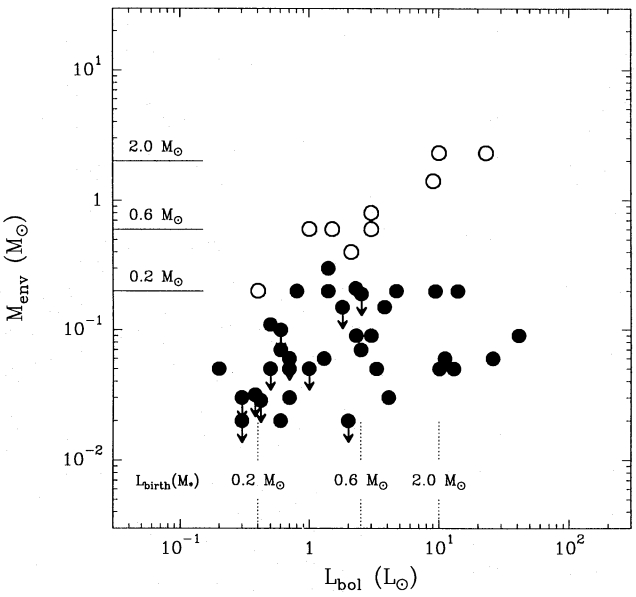

Fig. 1. Circumstellar envelope mass versus bolometric luminosity for the 45 YSOs surveyed for ^{12}CO(2–1) outflows (Class 0s and Class Is shown as open and filled circles, respectively). The range of envelope masses spanned by Class 0 sources is shown as interrupted horizontal solid lines. The range of birthline luminosities L_{birth} corresponding to three typical stellar masses (0.2, 0.6, and 2 $M_\odot$) are indicated as vertical dotted lines. The lowest L_{birth} (for 0.2 $M_\odot$) corresponds to $\dot{M}_{acc} = 2 \times 10^{-6}\,M_\odot yr^{-1}$, the highest one (for 2 $M_\odot$) is for $\dot{M}_{acc} = 10^{-5}\,M_\odot yr^{-1}$, while L_{birth}(0.6 $M_\odot$) does not strongly depend on $\dot{M}_{acc}$ (see Stahler 1988, and also Fletcher & Stahler 1994). This diagram suggests that our sample is representative of the protostellar evolution of young stars with typical mass $\sim 0.6\,M_\odot$

2. Observations

2.1. Source sample

The original goal of our CO(2–1) observations was to make a complete and homogeneous survey for molecular outflows in the Class I (and Class 0) sources of ρ Ophiuchi and Taurus-Auriga. This led to a study of 24 Class I and 4 Class 0 objects embedded in these two low-mass, nearby ($d \sim 150$ pc) star-forming regions. Our initial sample thus included all 16 YSOs classified as Class I or Class 0 by AM in ρ Ophiuchi (with the exception of the Class I source IRS54); these objects cover the L_{bol} range 0.5 $L_\odot$ (LFAM1) to 41 $L_\odot$ (EL29). In Taurus-Auriga, we observed 11 Class I and 2 Class 0 YSOs among the ~ 20 embedded YSOs known in this region (see e.g., Kenyon et al. 1993); we did not reobserve the 2 Class I outflow sources 04016+2610 (L1489) and L1551-IRS5 (see Myers et al. 1988 and Moriarty-Schieven & Snell 1988). Our Taurus sample spans a L_{bol} range from 0.2 $L_\odot$ (04158+2805) to 3.8 $L_\odot$ (04361+2547).

In order to avoid cloud-dependent biases, we then enlarged this initial sample by including several embedded YSOs in the

Table 1. 45 embedded YSOs surveyed in ^{12}CO(2–1) for molecular outflows

YSO Name (1)	Core Name (2)	Coordinates(B1950) α (3)	δ (4)	d pc (5)	L_{bol} $L_\odot$ (6)	M_{env} $M_\odot$ (7)	SED Class (8)	Ref. (9)
L1448-IRS3	L1448	$03^h22^m31^s.9$	30° 34′ 50″	300	10.0	2.3	0	1
L1448-C	L1448	$03^h22^m34^s.3$	30° 33′ 35″	300	9.0	1.4	0	1
03282+3035		$03^h28^m15^s.2$	30° 35′ 14″	300	1.5	0.6	0	2
B5-IRS1	B5	$03^h44^m31^s.8$	32° 42′ 34″	300	9.4	0.2	I	3
04108+2803b	L1495	$04^h10^m48^s.0$	28° 03′ 49″	140	0.7	0.03	I	3
04158+2805	L1495	$04^h15^m52^s.2$	28° 05′ 10″	140	0.2	0.05	I	4
04166+2706	B213	$04^h16^m37^s.8$	27° 06′ 29″	140	0.4	0.2	0	4
04169+2702	B213	$04^h16^m53^s.8$	27° 02′ 48″	140	1.4	0.2	I	4
04181+2655	B213	$04^h18^m06^s.4$	26° 55′ 01″	140	0.5	$\leq$ 0.05	I	4
04181+2654	B213	$04^h18^m06^s.9$	26° 54′ 04″	140	0.7	$\leq$ 0.06	I	4
04295+2251	L1536	$04^h29^m32^s.2$	22° 51′ 11″	140	0.6	0.07	I	3
04302+2247	L1536	$04^h30^m16^s.8$	22° 47′ 04″	140	0.3	$\leq$ 0.05	I	5
04361+2547	TMR-1	$04^h36^m09^s.8$	25° 47′ 28″	140	3.8	0.15	I	3
04365+2535	TMC1A	$04^h36^m31^s.2$	25° 35′ 56″	140	2.4	0.2	I	3
04368+2557	L1527	$04^h36^m49^s.5$	25° 57′ 16″	140	1.6	0.4	0	6
04381+2540	TMC1	$04^h38^m08^s.5$	25° 40′ 53″	140	0.7	0.05	I	3
04489+3032	L1513	$04^h48^m58^s.1$	30° 32′ 49″	140	0.3	$\leq$ 0.02	I	3
16191-1936	L1719B	$16^h19^m09^s.0$	-19° 36′ 25″	160	1.8	$\leq$ 0.15[a]	I	3
GSS30-IRS1	OphA	$16^h23^m20^s.0$	-24° 16′ 18″	160	26.0	0.06	I	7
LFAM1	OphA	$16^h23^m20^s.3$	-24° 16′ 06″	160	0.5	0.11	I	8
VLA1623	OphA	$16^h23^m25^s.0$	-24° 17′ 47″	160	1.0	0.6	0	9
WL12	OphC	$16^h23^m42^s.5$	-24° 28′ 04″	160	4.1	0.03	I	10
EL29	OphE	$16^h24^m07^s.7$	-24° 30′ 37″	160	41.0	0.09	I	10
WL6	OphB	$16^h24^m19^s.8$	-24° 23′ 08″	160	2.0	$\leq$ 0.02	I	10
IRS43	L1681B/OphF	$16^h24^m25^s.1$	-24° 34′ 10″	160	10.1	0.05	I	10
IRS44	L1681B/OphF	$16^h24^m26^s.1$	-24° 32′ 51″	160	13.0	0.05	I	10
IRS46	L1681B/OphF	$16^h24^m27^s.4$	-24° 32′ 36″	160	0.6	0.02	I	10
IRS48	ρOph	$16^h24^m35^s.5$	-24° 23′ 55″	160	11.1	0.06	I	10
IRS51	L1681B2/OphF	$16^h24^m37^s.6$	-24° 36′ 35″	160	1.3	0.06	I	10
16285-2355	L1709B	$16^h28^m34^s.6$	-23° 55′ 05″	160	1.4	0.3	I	3
IRS67	L1689S	$16^h28^m58^s.3$	-24° 50′ 20″	160	2.5	0.07	I	8
16293-2422	L1689N	$16^h29^m21^s.0$	-24° 22′ 16″	160	23.0	2.3	0	11
16442-0929	L260	$16^h44^m13^s.9$	-09° 29′ 59″	160	0.7	$\leq$ 0.05[a]	I	3
16445-1352[b]	L158	$16^h44^m33^s.7$	-13° 52′ 03″	160	0.4	$\leq$ 0.03	I	12
16445-1405	L162	$16^h44^m32^s.0$	-14° 05′ 31″	160	0.4	$\leq$ 0.03	I	13
18148-0440	L483	$18^h14^m50^s.6$	-04° 40′ 49″	200	14.0	0.2	I	6
19156+1906	L723	$19^h15^m42^s.0$	19° 06′ 55″	300	3.0	0.6	0	14
19345+0727	B335	$19^h34^m35^s.1$	07° 27′ 24″	250	3.0	0.8	0	14
20353+6742	L1152	$20^h35^m19^s.4$	67° 42′ 30″	440	3.3	0.05	I	3
20503+6006	L1082C	$20^h50^m19^s.5$	60° 06′ 40″	440	0.6	-	I	12
20520+6003	L1082A	$20^h52^m04^s.5$	60° 03′ 18″	440	3.0	0.09	I	3
20526+5958	L1082B	$20^h52^m41^s.0$	59° 58′ 19″	440	0.8	0.2	I	12
20597+6800	L1174	$20^h59^m42^s.1$	68° 00′ 12″	440	2.4	$\leq$ 0.2	I	12
21106+4712	B361	$21^h10^m40^s.9$	47° 12′ 01″	350	4.7	0.2	I	12
23238+7401	L1262	$23^h23^m48^s.7$	74° 01′ 08″	200	2.3	0.09	I	15

[a] L1719B and L260 are unresolved in the continuum at 1.3 mm, consistent with dust emission from a disk.
[b] This IRAS source 16445-1352 was suspected of being a cirrus rather than an embedded YSO by Beichman et al. (1986).
References: (1) Bachiller et al. 1991a; (2) Bachiller et al. 1991b; (3) Myers et al. 1987; (4) Kenyon et al. 1990; (5) Kenyon et al. 1993; (6) Ladd et al 1991; (7) Ward-Thompson 1993; (8) photometry from AM and Greene et al. 1994; (9) AWB; (10) Wilking et al. 1989; (11) Walker et al. 1986; (12) Beichman et al. 1986; (13) Parker 1991; (14) Davidson 1987; (15) Terebey et al. 1993.

same low-luminosity range ($L_{bol} < 50$ $L_\odot$) but belonging to other nearby ($d < 450$ pc) regions of star formation (e.g., Perseus) or isolated cloud cores. Objects belonging to regions more distant than $d = 450$ pc were not considered in order to minimize confusion and distance-dependent effects and to concentrate on low-mass YSOs. Table 1 lists the most common name of each source (Column 1), the name of the associated cloud core (Column 2), the source 1950 equatorial coordinates (Columns 3 and 4), along with its distance (Column 5), bolometric luminosity (Column 6, based on the reference listed in Column 9), envelope mass (Column 7), and evolutionary class (Column 8). In total, therefore, we made CO(2–1) maps towards 45 embedded YSOs, comprising 36 Class I and 9 Class 0 sources.

In a related, complementary study, 1.3 mm continuum observations have been obtained for all these objects using the IRAM 30 m telescope equipped with the MPIfR bolometers (AM; André, Cabrit et al., in prep.). Thirty-six of our 45 sources are detected at 1.3 mm and most of them show evidence for extended dust millimeter emission, as expected if they are "self-embedded" in a circumstellar envelope (see AM). (Note, however, that 2 sources, L1719B and L260, appear to be unresolved, consistent with 1.3 mm emission from a disk.) These results are in qualitative agreement with model predictions made in the framework of the "standard" protostar theory (e.g., Terebey et

al. 1984) which suggest that the millimeter continuum flux of protostellar sources should be dominated by emission from the envelope rather than from the disk, when observed at the resolution of the IRAM 30 m telescope (Terebey et al. 1993). The status of the 9 sources undetected at 1.3 mm (for which we give upper limits to M_{env}) is more uncertain: they may not be truly self-embedded.

The envelope masses (M_{env}) listed in Column 7 of Table 1 were derived from 1.3 mm maps by integrating the observed dust emission over a region typically $\sim$ 1′ in diameter (corresponding to $\sim$ 10^4 AU at d = 160 pc). A mass opacity $\kappa_{1.3}$ = 0.01 cm^2 g^{-1} was assumed (cf. AM), in agreement with recent models of the dust emissivity in protostellar envelopes (e.g., Ossenkopf & Henning 1994). The values of M_{env} listed in Table 1 should provide a good estimate of the total envelope mass for objects in clusters such as the ρ Ophiuchi core, but may represent only the "inner" envelope mass for more isolated protostars in regions such as Taurus (see Motte et al. 1995). However, even in the latter case, M_{env} should still be a useful evolutionary indicator since the mass contained within a given radius of the protostellar envelope is expected to decrease with time (see Terebey et al. 1993 and Galli 1995).

Our sample may not be completely unbiased and probably over-represents the true fraction of Class 0s to Class Is, which is estimated to be $\sim$ 10 % in a given star-forming region like the ρ Oph core (e.g., AM). However, it should be reasonably representative of the evolution of low-mass YSOs during the "self-embedded" protostellar phase. This is illustrated by Fig. 1 which plots circumstellar envelope mass as a function of bolometric luminosity for the 45 sources in our sample. Such a graph has been recently proposed as an evolutionary diagram for embedded YSOs (Saraceno et al. 1996; see also AM). While Reipurth et al. (1993) have shown that M_{env} is well correlated with L_{bol} for the majority of embedded YSOs (i.e., Class I sources, displayed here as filled circles), Class 0 sources (open circles) stand out in this diagram as objects with excess circumstellar envelope mass. The final (main-sequence) masses of our sources may be estimated based on two extreme assumptions. The first estimate is given by the range of envelope masses measured for the Class 0 objects in our sample (which are likely to have $M_{env} >> M_*$), assuming they will eventually accumulate all (or most) of their circumstellar material. This is shown by (interrupted) horizontal solid lines in Fig. 1. The second estimate is based on the other extreme assumption that the Class I sources of our sample have just reached the birthline for pre-main sequence stars (see Stahler 1988) and have no accretion luminosity. This is shown by vertical dotted lines in Fig. 1 which mark the birthline luminosities corresponding to three representative stellar masses. Both estimates suggest a similar range of (final) stellar masses between $\sim$ 0.2 M$_\odot$ to $\sim$ 2 M$_\odot$. We conclude that our sample is likely to span a range of evolutionary stages from young Class 0 protostar (typical age $\sim$ 10^4 yr based on statistical arguments, e.g., AM) to evolved Class I source close to the birthline (age $\sim$ 10^5 yr), with an estimated average stellar mass of $\sim$ 0.6 M$_\odot$.

We also note here that $\sim$ 90 % of our objects have luminosities between $\sim$ 0.5 and 15 L$_\odot$ (i.e., a luminosity span of only a decade and a half). This is in marked contrast with the sample discussed by Saraceno et al. (1996) which spans a much broader range of luminosities between $\sim$ 0.5 and $\sim$ 1000 L$_\odot$. This also contrasts with the sample analyzed by Cabrit & Bertout (1992; hereafter CB) which includes mostly Class 0 sources with well-developed outflows and spans 5 decades in luminosity, with a median value $\sim$ 90 L$_\odot$ significantly larger than ours. Compared with the Cabrit & Bertout sample, the present sample spans a broader range of evolutionary stages but a smaller range of stellar masses. The same remark applies to the comparison between our sample and the sample of Herbig-Haro exciting sources observed in the continuum at 1.3 mm by Reipurth et al. (1993).

2.2. *Observations*

Our CO(2–1) observations were carried out using three telescopes during five sessions: three sessions with the National Radio Astronomy Observatory (NRAO)[1] 12 m telescope (30″ beam at 1.3 mm) at Kitt Peak in 1991 January and April, and 1992 January, one session with the Caltech Submillimeter Observatory (CSO)[2] 10 m antenna (30″ beam at 1.3 mm) on Mauna Kea in 1992 June, and a final session at Pico Veleta with the IRAM 30 m telescope (12″ beam at 1.3 mm) in 1993 June. Our observing strategy was to make, in a systematic fashion, small (3×3 or 5×5) ^{12}CO(2–1) maps of the close environment of the target YSOs in the position switching mode (the OFF position, which was checked to be free of emission, was typically 30′ away from the nominal source position). The spatial step of the raster maps was typically 30″, except in the case of the IRAM observations for which we used a 10″ step. The spectral (velocity) resolution depended on the telescope used: 500 kHz (0.65 km s^{-1}) at NRAO, $\sim$ 300 kHz (0.40 km s^{-1}) at CSO, and 200 kHz (0.26 km s^{-1}) at IRAM. Typical 1σ sensitivities were between 0.1 and 0.4 K for the NRAO observations, and around 0.15 K for both the CSO and IRAM observations. Relative calibration of data taken during different sessions and/or with different telescopes was achieved by using observations of the classical CO calibrator IRC10216 (cf. Mauersberger et al. 1991) as well as repeated observations of some central source positions.

3. Results

3.1. *CO(2–1) survey data*

We used two criteria to systematically assign an outflow status to the YSOs in our sample. First, we made maps of the integrated CO emission in blue-shifted and red-shifted velocity intervals (see Fig. 2 and Fig. 3). The low-velocity bound of

[1] The National Radio Astronomy Observatory is operated by Associated Universities, Inc., under cooperative agreement with the National Science Foundation.

[2] The CSO is operated by the California Institute of Technology under funding from the NSF, Contract # AST-90-15755.

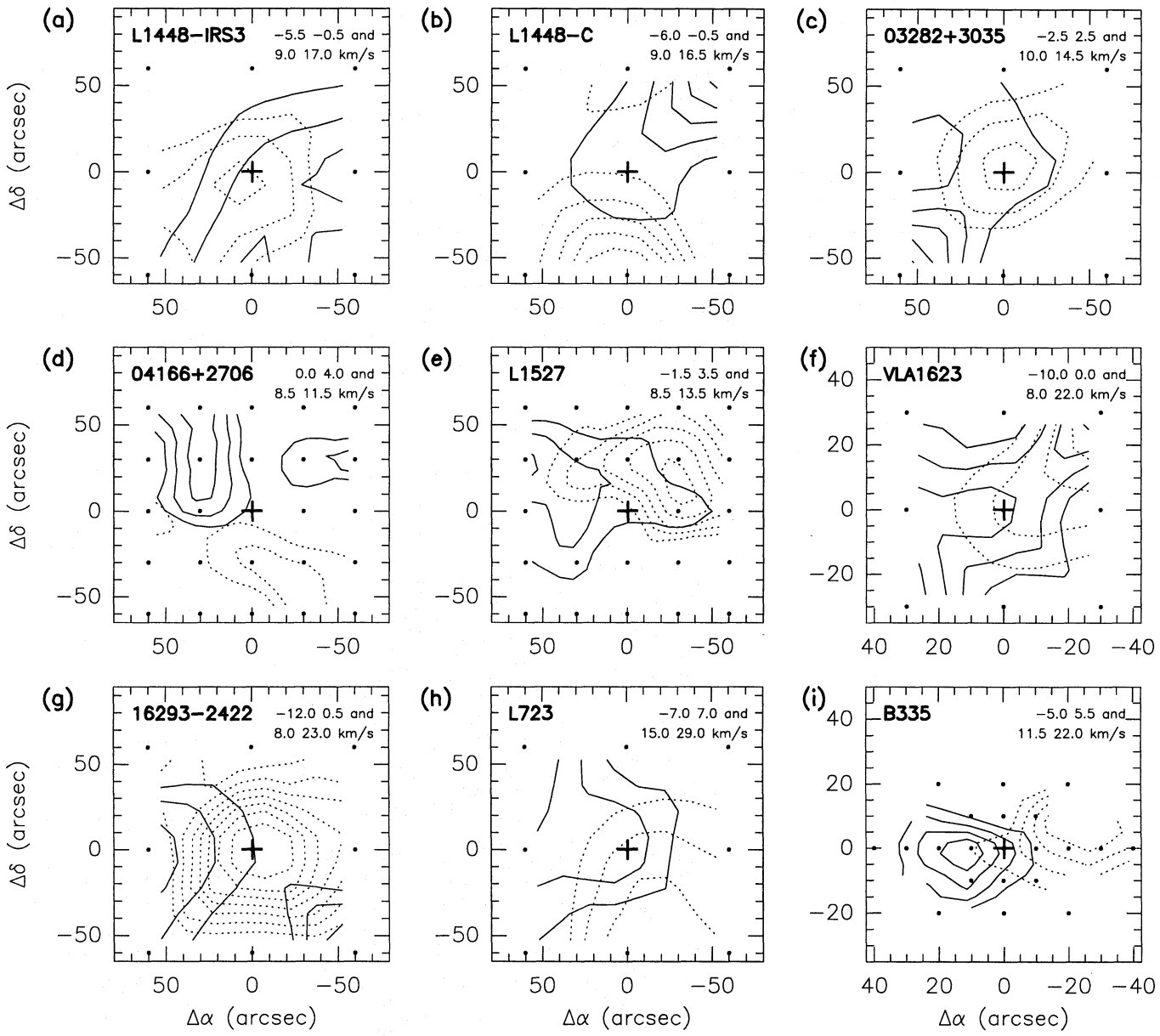

Fig. 2a–i. ^{12}CO(2–1) maps of the outflows from the 9 Class 0 sources in our sample; solid (resp. dashed) contours correspond to blue-shifted (resp. red-shifted) emission. Positions of central YSOs marked by crosses; blue- and red-shifted integration intervals indicated in upper left corners. Sources, lowest contours, and contour steps (for the blue- and red-shifted emission, respectively) are: **a** L1448-IRS3, (low 1.2, step 1.0) K.km s^{-1}(blue) and (low 2.0, step 1.0) K.km s^{-1} (red), **b** L1448C, (1.4, 1.0), (2.0, 1.0) K.km s^{-1}, **c** 03282+3035, (2.0, 0.5), (1.5, 0.5) K.km s^{-1}, **d** 04166+2706, (0.9, 0.3), (0.2, 0.3) K.km s^{-1}, **e** L1527, (0.9, 0.5), (1.4, 0.5) K.km s^{-1}, **f** VLA1623, (3.0, 1.5), (3.0, 1.5) K.km s^{-1}, **g** 16293-2422, (8.0, 5.0), (10.0, 5.0) K.km s^{-1}, **h** L723, (4.0, 1.5), (4.0, 1.5) K.km s^{-1}, **i** B335, (1.2, 0.7), (1.2, 0.7) K.km s^{-1}

each blue-shifted (resp. red-shifted) interval was chosen to be the velocity at which the "ambient" spectrum had $T_A^* = T_{peak}/10$ on the blue side (resp. red side). The high-velocity limits correspond to the velocities at which emission is no longer positively detected above the rms noise. This procedure is illustrated in Fig. 4 which shows a sample spectrum with its corresponding velocity intervals. Second, we subtracted a mean "off-source" spectrum from the "on-source" spectrum observed towards each source. The off-source spectrum was computed by averaging all spectra observed over a circle of angular radius $\theta \sim 15 - 70''$ (see Table 2) around the YSO position[3]. We then looked for excess emission at "high" velocities in the difference spectrum (see Fig. 4).

[3] This off-source spectrum may contain emission from high-velocity gas, especially in the case of a poorly collimated outflow seen pole-on. However, even in this case, we expect to see a contrast on source since outflow velocities are generally maximum on axis.

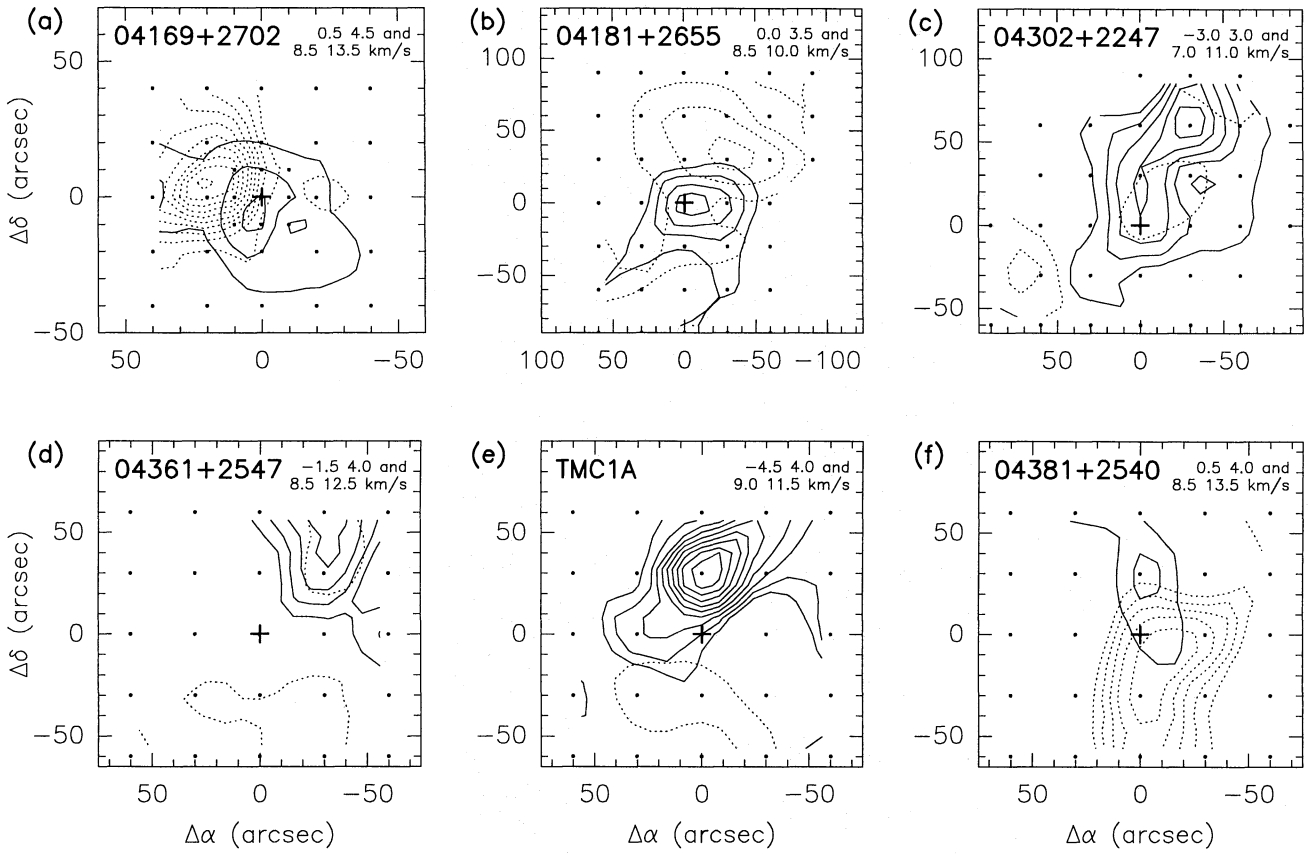

Fig. 3a–x. ^{12}CO(2–1) maps of the 24 outflows detected towards Class I sources; solid (resp. dashed) contours correspond to blue-shifted (red-shifted) emission. Positions of central YSOs marked by crosses; blue- and red-shifted integration intervals indicated in upper left corners. Sources, lowest contours, and contour steps (for the blue- and red-shifted emission, respectively) are: **a** 04169+2702, (low 0.4, step 0.5) K.km s^{-1}(blue) and (low 1.0, step 1.0) K.km s^{-1}(red), **b** 04181+2655, (0.4, 0.3), (0.3, 0.3) K.km s^{-1}, **c** 04302+2247, (0.7, 0.3), (0.6, 0.3) K.km s^{-1}, **d** 04361+2547, (1.2, 0.5), (0.7) K.km s^{-1}, **e** TMC1A, (1.0, 0.6), (0.7) K.km s^{-1}, **f** 04381+2540, (0.9, 0.4), (1.2, 0.4) K.km s^{-1}

We consider a given YSO to be an outflow source if the associated maps show a clear bipolar morphology or if the difference spectrum indicates excess emission at high velocities towards the central position. In this way, we classify 33 objects as outflow sources, which are listed in Table 2 along with the criterion used in each case ("b" and/or "w" for bipolar and wings, respectively). Eleven of these are new detections (outflow status labeled as "New"). Even though the velocities we observe are relatively low ($\sim$ 5 km s^{-1}), they are too high to be gravitationally-bound motions (see Terebey et al. 1992). Turbulence can also be excluded whenever a clear bipolar morphology is observed. The status of the 7 sources which fulfil only one of our outflow criteria is more uncertain than the other 26 outflow sources (L1719B, WL12, and L260 are the most uncertain detections; see Fig. 3). Three objects of the ρ Ophiuchi central region (GSS30-IRS1, LFAM1, and IRS46) cannot be assigned a reliable outflow status because of confusion with strong, nearby outflows. Only 9 objects out of 45 (04108+2803b, 04158+2805, 04181+2654, 04295+2251, 04489+3042, WL6, L158[4], L162, and L1082C) do not show any sign of outflow activity; they are listed as upper limits in Table 2. It is noteworthy that 6 of these 9 sources are undetected in the continuum at 1.3 mm and 8 have a bolometric luminosity lower than 0.7 $L_\odot$. The maps of all 33 detected outflows are shown in Fig. 2 (Class 0 YSOs) and Fig. 3 (Class I YSOs).

3.2. Outflow energetics

In order to study outflow energetics based on our limited but homogeneous set of CO observations (i.e., small $\sim 5\times5$ maps), we have estimated the momentum flux (or "force") along each flow. This dynamical quantity is better suited to our case than the momentum because it can be estimated even with incomplete maps of the flow. Since outflows from low-mass YSOs are thought to be momentum-driven (e.g., Masson & Chernin 1993), the combined momentum flux in all flow components (e.g., fast inner jet and "classical" slower CO flow) should be

[4] The IRAS source 16445-1352 in L158 is suspected of being a cirrus rather than an embedded YSO (Beichman et al. 1986). We therefore do not consider it in the discussion below.

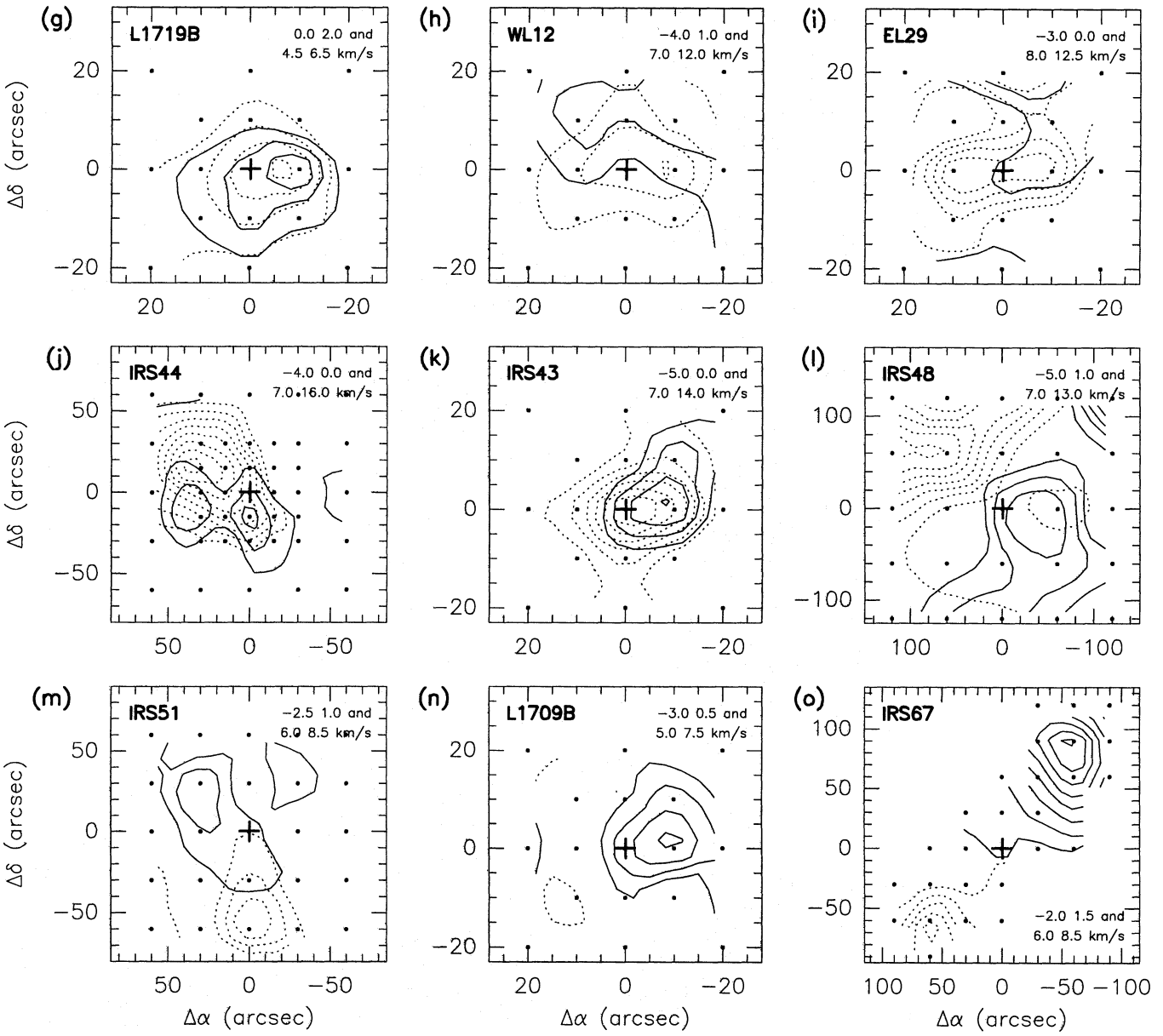

Fig. 3. g L1719B, contours are (low 0.3, step 0.2) K.km s^{-1}(blue) and (low 0.3, step 0.2) K.km s^{-1}(red), **h** WL12, (0.8, 0.5), (0.7, 0.5) K.km s^{-1}, **i** EL29, (0.8, 0.5), (1.3, 0.5) K.km s^{-1}, **j** IRS44, (1.4, 1.0), (2.2, 1.0) K.km s^{-1}, **k** IRS43, (0.9, 0.5), (0.9, 0.5) K.km s^{-1}, **l** IRS48, (2.0, 0.5), (2.0, 1.0) K.km s^{-1}, **m** IRS51, (1.2, 0.4), (1.2, 0.4) K.km s^{-1}, **n** L1709B, (0.8, 0.4), (1.0) K.km s^{-1}, **o** IRS67, (1.5, 1.0), (1.2, 1.0) K.km s^{-1}

conserved along the flow direction. If we ignore possible extremely high-velocity (EHV) components in young molecular outflows (which may correspond to momentum deposition relatively far from the central source), we can thus get reasonable estimates of the outflow momentum flux by using only CO observations obtained at a small distance from the central source (e.g., Raga et al. 1993). Another advantage is that the close environment of YSOs is likely to be less source-dependent than the remote environment.

In practice, we estimated the CO momentum flux $F_{\rm obs}$ across a surface perpendicular to the ouflow direction by integrating the observed momentum within a projected annulus (centered on the driving source) of radius r and width Δr, and dividing it by the apparent crossing time of the annulus, $\Delta r/v_{\rm rad}$. (This annulus thus defines a "slice" through the outflow.) The corresponding relation is:

$$F_{\rm obs} \propto \int_{\rm wings} \frac{T_{\rm A}^{*}(v_{\rm rad}){\rm d}v_{\rm rad}\, Area(r,\Delta r)\, v_{\rm rad}}{\Delta r/v_{\rm rad}}, \qquad (1)$$

where $Area(r, \Delta r) \propto r\,\Delta r$. It can be seen that expression (1) above is independent of Δr and thus provides an estimate of the local CO momentum flux $F_{\rm obs}(r)$. The actual prescription used was systematic but the values of r and Δr vary with telescope and mapped area (see Column 3 of Table 2). In particular, the

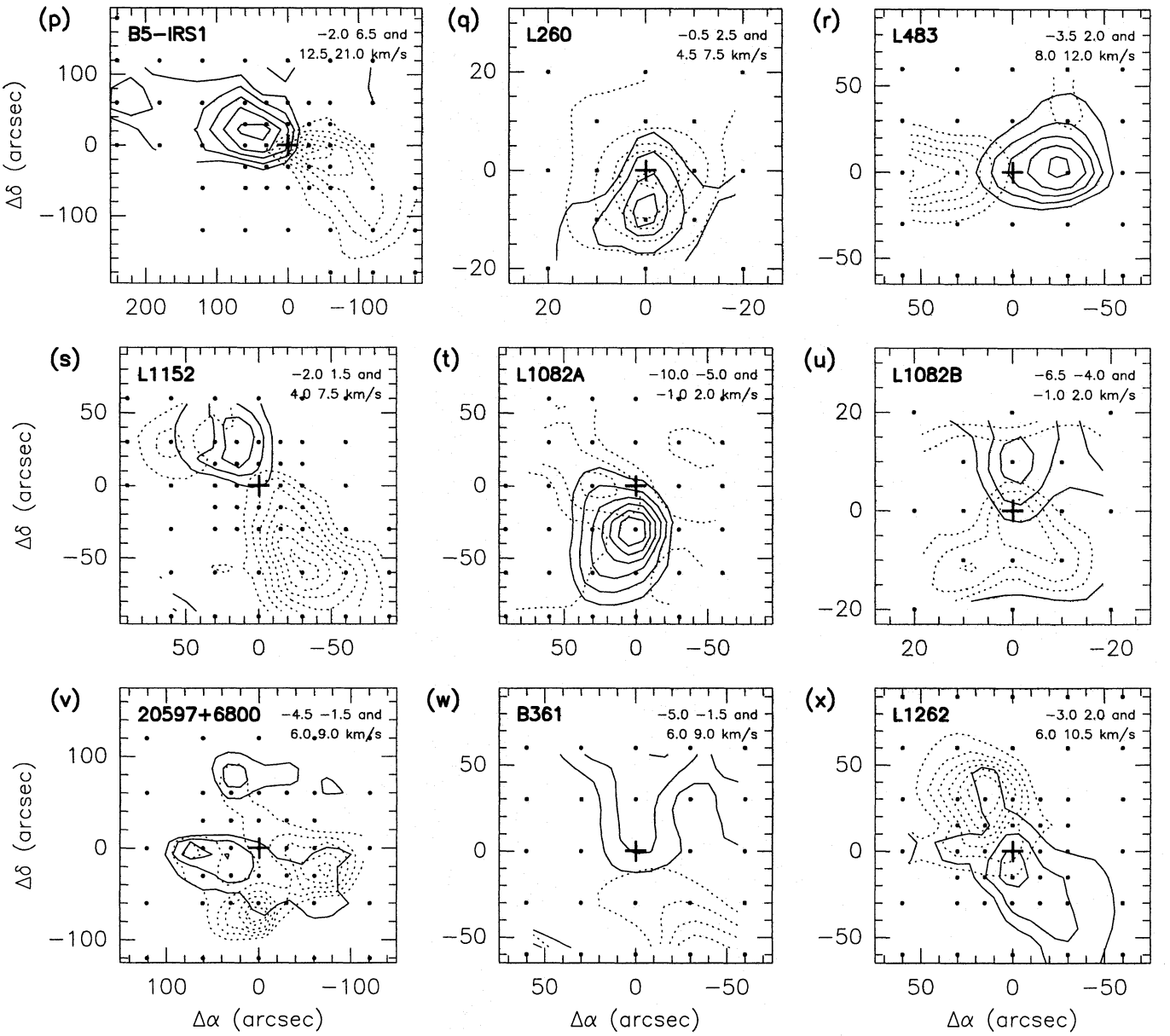

Fig. 3. p B5-IRS1, contours are (low 1.0, step 0.5) K.km s^{-1}(blue) and (low 1.2, step 0.5) K.km s^{-1}(red), **q** L260, (0.3, 0.2), (0.3, 0.2) K.km s^{-1}, **r** L483, (1.6, 1.0), (1.7, 1.0) K.km s^{-1}, **s** L1152, (0.5, 0.5), (1.0, 0.5) K.km s^{-1}, **t** L1082A, (1.0, 0.5), (0.5, 0.5) K.km s^{-1}, **u** L1082B, (0.4, 0.2), (0.7, 0.2) K.km s^{-1}, **v** 20597+6800, (0.5, 0.3), (0.7, 0.3) K.km s^{-1}, **w** B361, (0.6, 0.3), (0.6, 0.3) K.km s^{-1}, **x** L1262, (1.0, 1.0), (1.0, 1.0) K.km s^{-1}

annular radius r was adapted to the spatial coverage in order to ensure a good sampling of the ring of integration in all cases.

The resulting estimates $F_{\rm obs}$ do not take projection or optical depth effects into account. If i is the inclination angle between the flow axis and the line of sight, the actual thickness of the "slice" is $\Delta r/\sin i$, while the actual flow velocity is $v_{\rm rad}/\cos i$. This leads to an inclination correction factor $f(i) = \frac{\sin i}{\cos^2 i}$ for the CO momentum flux. Lacking complete CO maps, we cannot estimate the inclination angle i on an individual basis, and therefore use a mean correction factor $< f(i) > = 2.9$ corresponding to a mean inclination angle $i_0 \approx 57.3°$ (assuming random outflow orientations). As to the opacity correction $\frac{\tau_{\rm CO}}{1-e^{-\tau_{\rm CO}}}$ (where $\tau_{\rm CO}$ is the mean line optical depth), we adopt the same mean factor of 3.5 as CB in their detailed investigation of uncertainty effects on molecular outflow parameters. Therefore, our best estimate of the corrected CO momentum flux is:

$$F_{\rm CO} = < f(i) > \times < \frac{\tau_{\rm CO}}{1-e^{-\tau_{\rm CO}}} > \times F_{\rm obs} \sim 10 \times F_{\rm obs}, \qquad (2)$$

which is the quantity we use in the following sections. This value of $F_{\rm CO}$ is listed for each detected outflow in Column 5 of Table 2, along with the uncertainty due to spectrum noise; 3σ upper limits are provided for undetected outflows.

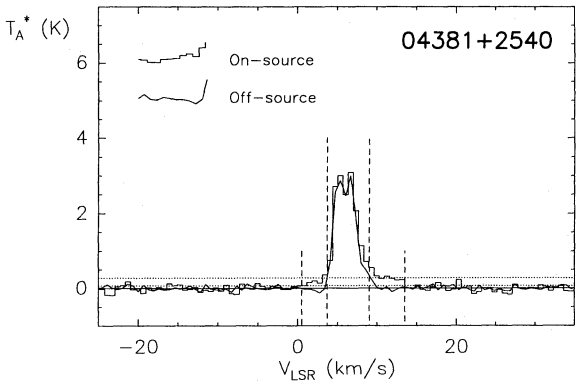

Fig. 4. Excess emission in the high-velocity wings towards 04381+2540 (in TMC1) observed at NRAO. We find a $\Delta v_{1\sigma} \sim 13\,\mathrm{km\,s^{-1}}$. The spectrum observed on-source is shown as an histogram line, and the off-source spectrum, obtained by averaging all the spectra at $\sim 45''$, as a smooth line. The vertical, dashed lines show the velocity bounds used to search for excess emission at high-velocity (see text)

Our estimates of F_{CO} agree well with previous determinations of the momentum flux when these did not take EHV components into account. In particular, our values lie within a factor of $2-3$ of the CB estimates, with no systematic offset (see also Sect. 3.2.1). The same is true when we compare with the measurements of Goldsmith et al. (1984, 1986) (for B5-IRS1, L723, and B335), Terebey et al. (1989) (for IRS44), and Parker et al. (1991) (for L483 and L1262). In contrast, our estimates are systematically lower, by a factor of $\sim 3-5$, than recent measurements which include EHV CO components (see Bachiller et al. 1990, 1991b and André et al. 1990 for L1448C, 03282+3035, and VLA1623, respectively). This suggests that our method of measuring F_{CO} is adequate for "classical" outflows[5] but may underestimate the energetics of EHV flows from some Class 0 sources.

3.2.1. Correlation with L_{bol}

Fig. 5 plots the CO momentum flux F_{CO} against the bolometric luminosity L_{bol} of the driving source. The two evolutionary classes of self-embedded YSOs are shown by different symbols: open circles for Class 0 sources and filled circles for Class I YSOs.

Although our sample spans only a small range of luminosities (e.g., Sect. 2.1), a significant overall correlation is apparent in this plot. Using the ASURV[6] statistical package, we estimate that the probability of no correlation is lower than 0.01 % (corresponding to a positive correlation at the 4.8 σ level). However, Class 0 objects appear to be outliers: they drive systematically more powerful CO outflows than Class Is of similar luminosities. This is a clear quantitative evidence of the fact already noted

Table 2. Outflow status and observed CO momentum flux for our 45 YSOs

Adopted Name (1)	Telescope(s) Used (2)	θ, $\Delta\theta$[a] (arcsec) (3)	Outflow Status[b] (4)	F_{CO}[c] ($10^{-5}M_\odot$ km s^{-1}yr^{-1}) (5)
L1448-IRS3	NRAO	70, 30	b & w	10 ± 1.9
L1448-C	NRAO	70, 30	b & w	14 ± 2.9
03282+3035	NRAO	70, 30	b & w	6.8 ± 1.1
B5-IRS1	NRAO	45, 30	b & w	4.1 ± 0.07
04108+2803b	NRAO		No	≤ 0.16
04158+2805	NRAO		No	≤ 0.23
04166+2706	NRAO	45, 30	b & w, New	0.31 ± 0.10
04169+2702	IRAM	20, 12	b & w	0.57 ± 0.02
04181+2655	NRAO	45, 30	b & w, New	0.22 ± 0.05
04181+2654	NRAO		No	≤ 0.14
04295+2251	NRAO		No	≤ 0.18
04302+2247	NRAO	45, 30	b & w	0.31 ± 0.09
04361+2547	NRAO	45, 30	w	0.61 ± 0.07
TMC1A	NRAO	45, 30	b & w	1.6 ± 0.10
L1527	NRAO	45, 30	b & w	0.79 ± 0.13
04381+2540	NRAO	45, 30	b & w	0.57 ± 0.12
04489+3042	NRAO		No	≤ 0.11
L1719B	NRAO/IRAM	15, 12	w, New	0.04 ± 0.003
GSS30IRS1[d]	IRAM		-	-
LFAM1[d]	IRAM		-	-
VLA1623	NRAO/CSO	35, 30	b & w	14 ± 0.28
WL12	NRAO/IRAM	15, 12	w, New	0.6 ± 0.06
EL29	NRAO/IRAM	15, 12	b & w, New	1.5 ± 0.14
WL6	NRAO		No	≤ 1.5
IRS43	NRAO/IRAM	15, 12	w, New	1.5 ± 0.12
IRS44	NRAO/CSO	45, 30	b & w	2.7 ± 0.31
IRS46[e]	CSO		-	-
IRS48	NRAO	90, 30	b & w, New	3.0 ± 0.61
IRS51	CSO	45, 30	b & w, New	0.55 ± 0.18
L1709B	NRAO/IRAM	15, 12	w	0.63 ± 0.02
IRS67	CSO	70, 30	b	1.0 ± 0.13
16293-2422	CSO	70, 30	b & w	42 ± 0.74
L260	CSO/IRAM	15, 12	w	0.03 ± 0.002
L158[f]	CSO		No	≤ 0.09
L162	CSO		No	≤ 0.06
L483	CSO	45, 30	b & w	1.5 ± 0.37
L723	NRAO	70, 30	b & w	37 ± 0.33
B335	IRAM	15, 12	b & w	1.2 ± 0.05
L1152	CSO	45, 30	b & w, New	0.47 ± 0.10
L1082C	CSO		No	≤ 0.72
L1082A	NRAO	45, 30	b & w, New	2.5 ± 0.29
L1082B	CSO/IRAM	15, 12	b & w, New	0.28 ± 0.03
20597+6800	NRAO	45, 30	b & w	2.8 ± 0.50
B361	CSO	45, 30	b & w	1.5 ± 0.46
L1262	CSO	45, 30	b & w	1.1 ± 0.08

[a] Angular radius θ and width $\Delta\theta$ of the annulus used to estimate F_{CO} (see text). For 3×3 maps sampled every 60″, θ is the mean distance of the 8 off-source spectra (i.e. $\sim 70''$); for 5×5 maps sampled every 30″, θ is $\sim 45''$; for 5×5 maps sampled every 10″, θ is $\sim 15''$. $\Delta\theta$ is always equal to the beam FWHM (12″ or 30″).

[b] Outflow status: "b" for bipolar morphology, "w" for high-velocity wings, and "New" for new detections.

[c] $F_{CO} \sim 10 \times F_{obs}$ after correction for inclination and optical thickness of ^{12}CO(2–1) (see Sect. 3.2).

[d] Confusion with the CO outflow from VLA1623 prevents measurements for these sources.

[e] IRS46 is confused by the CO outflow from IRS44.

[f] The IRAS source is probably a cirrus (see text and Table 1).

[5] Since we measure F_{CO} at a typical distance of 0.06 pc (i.e., 1′ at 200 pc) from the central source, in a slice of width $\sim$ 0.03 pc (30″ at 200 pc), the "smoothing time" associated with our measurements is of the order of 0.05 pc/5 km s^{-1} $\sim 10^4$ yr. On the other hand, the smoothing time of classical determinations is on the order of the outflow apparent dynamical timescale (typically $\gtrsim 10^4$ yr in our sample of low-luminosity sources) (see Masson & Chernin 1993). Therefore, both methods yield F_{CO} values which correspond to averages over a time short compared to the entire outflow lifetime ($\gtrsim 10^5$ yr, see Sect. 4.1).

[6] ASURV (rev 1.2) is a software package which implements "survival analysis" techniques and is well suited to statistical analysis of astronomical data including upper limits (e.g. Feigelson & Nelson 1985, Isobe et al. 1986).

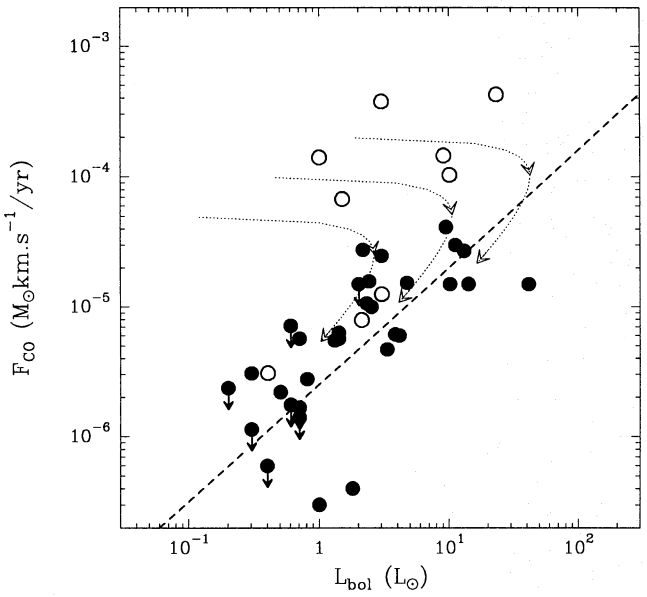

Fig. 5. CO momentum flux F_{CO} versus bolometric luminosity L_{bol} for the 41 sources for which we have estimated F_{CO} (Class 0s and Class Is shown as open and filled circles, respectively). The 'best fit' F_{CO}–L_{bol} correlation found for Class I sources is plotted as a dashed line. The dotted curves represent indicative evolutionary tracks illustrating the 'toy' model proposed in Sect. 4.3.1, for three initial envelope masses (0.3, 0.6, and 1.2 $M_\odot$, from left to right). Arrows are shown on the tracks at t = ln 2 × τ ∼ 6 × 10^4 yr and t = ln 10 × τ ∼ 2 × 10^5 yr, when 50 % and 90 % of the initial envelope mass have been accreted, respectively ($\tau \sim 9 \times 10^4$ yr is the characteristic time of the model)

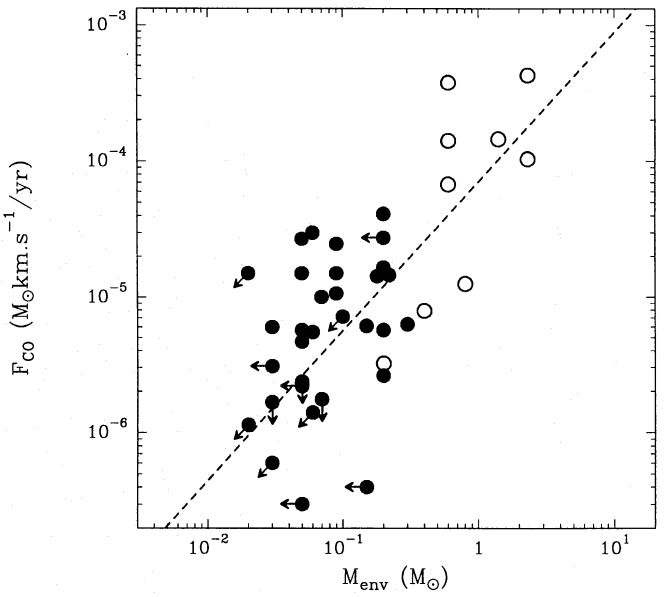

Fig. 6. CO momentum flux versus circumstellar envelope mass. Class 0 YSOs are plotted as open circles and Class I YSOs as filled circles. The 'best fit' F_{CO}–M_{env} correlation for the entire sample is plotted as a dashed line. In contrast to Fig. 5, Class 0s here follow the same correlation as Class Is

by some authors (e.g., Bachiller et al. 1991a; AWB) that Class 0 protostars are more efficient than Class I sources at driving their outflows.

For Class Is alone, we find that the best fit for the significant (4.6 σ) linear correlation between log(F_{CO}) and log(L_{bol}) is:

$$\log\left(F_{CO}/M_\odot \mathrm{km\ s^{-1}yr^{-1}}\right) = -(5.6 \pm 0.1) + (0.9 \pm 0.15)\ \log\left(L_{bol}/L_\odot\right) \quad (3)$$

Since the slope of this log–log correlation is ∼ 1, there is also a linear relationship between F_{CO} and L_{bol}, expressing the fact that Class I sources all have about the same outflow efficiency $F_{CO}/F_{rad} \sim 100$, (where $F_{rad} = L_{bol}/c$ is the radiative momentum flux). For Class 0 sources alone, we do not find a significant correlation owing to the small number of objects (9), but we estimate that they have an outflow efficiency $F_{CO}\,c/L_{bol} \sim 1000$, on average. They thus lie a factor of ∼ 10 above the Class I correlation in Fig. 5.

We stress that the higher outflow efficiency estimated for Class 0 sources does not result from a bias towards large viewing angles for these objects. A very large inclination angle i (i.e., a source viewed close to edge-on) may lead to a significant underestimate of L_{bol} for a source surrounded by a protostellar disk (e.g., Yorke et al. 1995). However, estimates of i exist for 6 of the 9 Class 0s in our sample (CB), and only 2 of them have $i > 70°$ (the other 4 having $i < i_0 = 57.3°$). Furthermore, a large value of i also leads to an underestimate of F_{CO} (cf. Eq. (2) above), so that the two effects tend to cancel in $F_{CO}\,c/L_{bol}$.

Our results on the F_{CO}–L_{bol} correlation agree well with previous works obtained on samples which cover several decades in luminosity: Rodríguez et al. (1982), Bally & Lada (1983), Lada (1985), Levreault et al. (1988), Mozurkewich et al. (1986) found correlation slopes around 0.8 – 0.9 and efficiencies typically in the range 100 – 1000. The most recent work by CB found a slope of 0.69 ± 0.05 and an efficiency ∼ 250 (at 1000 $L_\odot$) for their entire sample, while at low luminosity (L_{bol} a few $L_\odot$) the slope was higher ∼ 0.9 – 1.0 and the efficiency was ∼ 1000 (see their Fig. 1). Our results are thus in excellent agreement with the measurements of CB, especially for Class 0 sources in the same L_{bol} range. This is not surprising since the CB sample is focused on well-collimated flows, and therefore contains a majority of Class 0 sources (6 of them, L1448-C, 03282+3035, VLA1623, 16293-2422, L723, and B335, being also in our sample).

3.2.2. Correlation with M_{env}

Fig. 6 plots our estimate of the CO momentum flux F_{CO} against the circumstellar envelope mass M_{env} for each source in our sample. As in Figs. 1 and 5, Class 0 and Class I sources are plotted as open and filled circles, respectively. There appears to be a good correlation between F_{CO} and M_{env}, in agreement with the difference between Class 0s and Class Is pointed out in the previous section. Survival analysis indicates that the correlation is significant at the 4.8 σ level (i.e., a probability of no correlation lower than 0.01 % and comparable to that found in Sect. 3.2.1 for F_{CO} versus L_{bol}). We find that the best-fit linear relationship

between $\log(F_{CO})$ and $\log(M_{env})$ is:

$$\log\left(F_{CO}/M_{\odot}\mathrm{km\ s^{-1}yr^{-1}}\right) = -(4.15 \pm 0.1) + (1.1 \pm 0.15)\log\left(M_{env}/M_{\odot}\right) \quad (4)$$

A similar correlation, between CO outflow mechanical luminosity and sub-millimeter 800 μm continuum flux density, was recently pointed out by Moriarty-Schieven et al. (1994), who found $L_{CO} \propto {F_{800}}^{1.9\pm0.5}$. Our present study agrees with their results but points to a lower power-law index, closer to ~ 1 than ~ 2. Although seven objects are common to both studies, we cannot further compare our respective results because Moriarty-Schieven et al. used the surrogate quantity $\int T_A^* (\Delta V_{av})^3\, dv$ evaluated in a single spectrum at the central source, instead of a direct estimate of the outflow mechanical luminosity based on a CO map.

4. Discussion

4.1. Frequency of occurrence of outflows

Assuming our sample is representative (see Sect. 2.1), the results of our CO survey imply a very high frequency of outflows during the *self-embedded* phase of low-mass YSOs: $33-36$ of the 44 YSOs in the entire sample show outflow activity, i.e., a detection rate of $\sim 75-80$ %; among the 34 YSOs with positively detected extended dust continuum emission, the outflow detection rate is even higher, reaching $\sim 80-90$ % (see Table 1). Furthermore, all 8 YSOs with no evidence of outflow activity lie near the lower end of the luminosity range and have among the weakest millimeter continuum emission of the sample (see Sect. 3.1). We conclude that probably *all* low-mass YSOs still embedded in a significant circumstellar envelope drive a molecular outflow, which confirms and strengthens the results of previous CO outflow surveys of embedded YSOs (e.g., Heyer et al. 1987, Myers et al. 1988, Terebey et al. 1989, Parker et al. 1991). This implies that the duration of the outflow phase is comparable to the typical lifetime of Class I sources, i.e., $\sim 2\times10^5$ yr (e.g., Greene et al. 1994). As noted by Parker et al. (1991), the duration of the CO outflow phase is significantly longer than the typical dynamical timescale measured for the high-velocity gas. In our case, the dynamical timescale of the observed high-velocity gas is typically $\sim 10^4$ yr, taking a characteristic outflow velocity of 5 km s^{-1} at a distance of ~ 0.05 pc (i.e., 50″ at $d = 200$ pc) from the central source; this is only $\sim 1/20$ of the estimated outflow phase duration.

It is noteworthy that our study indicates a very high outflow occurrence even in the dense, central region of the ρ Ophiuchi cloud, where previous unsuccessful searches (e.g., Fukui et al. 1986) had led to the suggestion that outflows may be inhibited by an unusually high density. According to AM, there are 11 Class I YSOs with $L_{bol} > 1\ L_{\odot}$ in the central ρ Oph core, and only one Class 0 source (i.e., VLA 1623). We have CO data for all these self-embedded YSOs except IRS54. Three of them are confused by outflows from other objects (LFAM1, GSS30-IRS1, and IRS46). We find outflows around 7 of the remaining 8 objects, of which 5 are new detections. Most of these new outflows are spatially more compact and more than an order of magnitude less energetic than the well-developed outflows driven by the 2 Class 0 YSOs known in the ρ Ophiuchi cloud (i.e., VLA1623 and 16293-2422, the latter being in L1689 eastward of the ρ Ophiuchi central core). This, coupled with the fact that the CO line from the ambient cloud is particularly broad in this region, most likely explains why these outflows had not been detected in previous studies. More generally, our results agree well with the suggestion by Terebey et al. (1989) that there exists a population of compact molecular outflows around low-luminosity "IRAS dense cores".

4.2. Decline of CO outflow energetics with evolutionary stage

We have shown in Sect. 3.2 that the outflow momentum flux is well correlated both with the bolometric luminosity (for Class I sources) and with the circumstellar envelope mass (for Class I and Class 0 sources). Interpreting these correlations is critical to understanding the origin of outflows and the significance of outflow activity in the star formation process. The correlation of outflow energetics with bolometric luminosity has already been extensively discussed by several authors (e.g., Lada 1985, Levreault 1988, Bally & Lane 1991). These previous studies suggested three main conclusions: (1) the driving engine mechanism is likely to be similar for all sources, (2) outflow energetics is mainly determined by the luminosity of the central source (presumably deriving mostly from accretion), and (3) outflows cannot be accelerated by radiation pressure.

Most remarkable is the tight correlation we find between the outflow momentum flux F_{CO} and the circumstellar envelope mass M_{env}: F_{CO} is roughly proportional to M_{env} in our sample (see Sect. 3.2.2 and Fig. 6). As explained in Sect. 1 and Sect. 2.1, the variations of M_{env} in our sample most likely reflect a range of evolutionary stages from young Class 0 protostars with large M_{env} (on the right-hand side of Fig. 6) to evolved Class I protostars with small M_{env} (on the left-hand side of Fig. 6). Therefore, Fig. 6 suggests a decrease of CO outflow energetics with evolutionary stage, from Class 0 to Class I.

More quantitatively, using the ASURV statistical package to estimate the (geometric) mean properties of Class 0 and Class I sources in our sample, we find systematic differences in both M_{env} and F_{CO} between the two evolutionary classes: on average, the circumstellar envelope mass and the outflow momentum flux are both an order of magnitude larger for Class 0s (geometric means $< M_{env} >= 0.8\,M_{\odot}$ and $< F_{CO} >= 5.7\times10^{-5}\,M_{\odot}\mathrm{km\ s^{-1}yr^{-1}}$) than for Class Is ($< M_{env} >= 0.06\,M_{\odot}$, and $< F_{CO} >= 3.8\times10^{-6}\,M_{\odot}\mathrm{km\ s^{-1}yr^{-1}}$); these differences are significant at the 6.8 σ level and 3.7 σ level, respectively. In contrast, the average bolometric luminosity is similar for both classes ($< L_{bol} >= 3.1\,L_{\odot}$, and $< L_{bol} >= 1.9\,L_{\odot}$ for Class 0s and Class Is, respectively, with a probability of identical distributions of ~ 55 %). We conclude that the decrease of F_{CO} and M_{env} from Class 0 to Class I (e.g., Fig. 6) is primarily an evolutionary effect rather than a YSO luminosity (or stellar mass) effect.

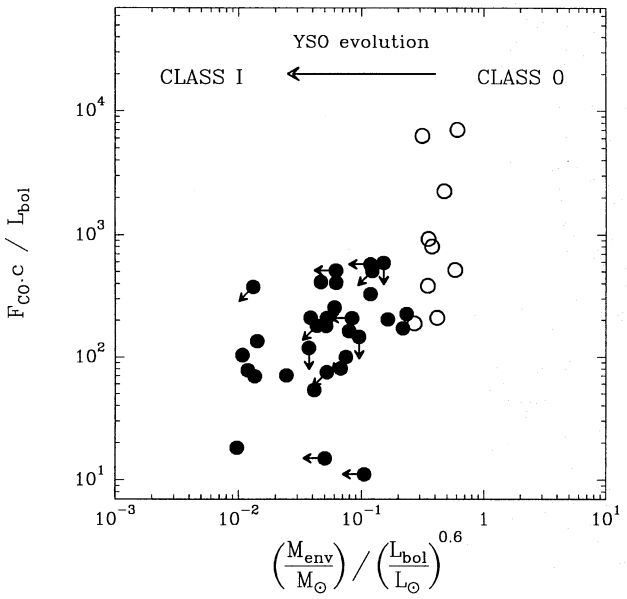

Fig. 7. $F_{CO}\,c/L_{bol}$ (dimensionless) versus $M_{env}/{L_{bol}}^{0.6}$ (M_{env} and L_{bol} in units of $M_\odot$ and $L_\odot$) for the 41 YSOs discussed in Sect. 4. Class 0 YSOs are plotted as open circles and Class I YSOs as filled circles. This diagram which should be almost free of any luminosity and distance effects provides clear evidence for a decline of outflow strength from Class 0s to Class Is (see text)

To further support this interpretation and emphasize evolutionary trends, we have tried to remove any luminosity dependence from both F_{CO} and M_{env}. Since we find $F_{CO} \propto {L_{bol}}^{1.04\pm0.2}$ (cf. Fig. 5) and $M_{env} \propto {L_{bol}}^{0.56\pm0.2}$ (cf. Fig. 1) in our entire sample, we plot the outflow efficiency $F_{CO}\,c/L_{bol}$ versus $M_{env}/{L_{bol}}^{0.6}$ in Fig. 7. This figure, which should be almost free of any luminosity and distance effects, clearly indicates a decline of outflow efficiency with evolutionary stage: $F_{CO}\,c/L_{bol}$ goes from $\sim$ 3000 for young Class 0 sources to $\sim$ 70 for the most evolved Class Is.

We note that Fig. 7 suggests a break in outflow efficiency between Class 0s and Class Is, in agreement with the idea that the outflows from these two classes of protostars have qualitatively different properties (see also AWB). One possibility is that outflows from Class 0 sources primarily reflect a single ejection event, while Class I flows result from the averaged action of many jet episodes (see also Chernin & Masson 1995 and Sect. 4.3.2 below). On the other hand, the tight correlation seen in Fig. 6 points to a smooth decrease of F_{CO} with M_{env}, with no particular discontinuity between Class 0s and Class Is. A similar trend has been noted by Saraceno et al. (1996) on a sample of embedded YSOs spanning a broader range of luminosities. This suggests that F_{CO} may primarily depend on only one basic parameter related to M_{env}, rather than separately on age and stellar mass (see also Sect. 4.3.1 below).

4.3. Interpretation of the observed evolution of CO outflow activity

It is now widely believed that CO outflows are momentum driven by a jet/wind originating in the innermost regions of the circumstellar disk/envelope of protostars (e.g., Königl & Ruden 1993). The most plausible energy source for this jet/wind is the gravitational energy released by infall and/or accretion onto the protostar. In this view, CO outflows are related to accretion through two main steps: the ejection mechanism which produces the jet/wind, and the entrainment process which builds observed outflows from ambient molecular gas. Accordingly, the CO outflow momentum flux may be expressed as a function of the accretion rate $\dot{M}_{acc}$:

$$F_{CO} = f_{ent} \times (\dot{M}_w/\dot{M}_{acc})\, V_w \times \dot{M}_{acc}, \quad (5)$$

where the entrainment efficiency f_{ent} is the factor relating F_{CO} to the momentum flux $F_w = \dot{M}_w\, V_w$ of the wind at its source (i.e., before any interaction with ambient gas). A priori, the observed decline of F_{CO} with evolutionary stage may thus result from a decrease of $\dot{M}_{acc}$, which we discuss in Sect. 4.3.1, or from a decrease of one of the other two factors entering Eq. (5), which we discuss in Sect. 4.3.2.

4.3.1. A decline of the mass accretion rate ?

Assuming an entrainment efficiency $f_{ent} = 1$ and a typical wind/jet velocity $V_w \sim 150$ km s^{-1}, the decrease in $F_{CO} = f_{ent}\,\dot{M}_w\,V_w$ seen in Fig. 6 suggests a decrease of the wind/jet mass-loss rate $\dot{M}_w$ from $\sim 1.2 \times 10^{-6}\,M_\odot yr^{-1}$ for the youngest Class 0 sources (corresponding to $L_{bol} = 3\ L_\odot$, and $F_{CO}c/L_{bol} = 3000$ in Fig. 7) to $\sim 2 \times 10^{-8}\,M_\odot yr^{-1}$ for the most evolved Class I sources ($L_{bol} = 2\ L_\odot$, and $F_{CO}c/L_{bol} = 70$).

In the case of classical T Tauri stars, diagnostics for $\dot{M}_w$ and $\dot{M}_{acc}$ (such as the [OI] forbidden line luminosity and the mid-IR excess luminosity) are found to correlate very well with each other (e.g., Cabrit et al. 1990, Edwards et al. 1993, Hartigan et al. 1995). Furthermore, many of the theoretical models proposed to explain the powering mechanism of YSO jets/outflows predict a direct proportionality between $\dot{M}_w$ and $\dot{M}_{acc}$. It is therefore tempting to conclude that the above decrease in F_{CO} and $\dot{M}_w$ traces a corresponding *decline in mass accretion and/or infall rate*. The calculations of Shu et al. (1994) suggest a ratio $\dot{M}_w/\dot{M}_{acc}$ between 0.1 and 0.5, Pelletier & Pudritz (1992) propose $\dot{M}_w/\dot{M}_{acc} \sim 0.1$ from their models, and Wardle & Königl (1993) find solutions with $\dot{M}_w/\dot{M}_{acc}$ ranging from 10^{-5} to 10^{-1}. Adopting $\dot{M}_w/\dot{M}_{acc} = 0.1$, we estimate that $\dot{M}_{acc}$ should decrease from $\sim 10^{-5}\,M_\odot yr^{-1}$ to $\sim 2 \times 10^{-7}\,M_\odot yr^{-1}$ to account for the observed evolution of outflow energetics through the self-embedded phase.

Based on the tight correlation observed between F_{CO} and M_{env} (Fig. 6), we may go further and propose a more detailed description of the decrease of $\dot{M}_{acc}$ with time. Fig. 6 suggests $F_{CO} \propto M_{env}$, which in turn implies $\dot{M}_{acc} \propto M_{env}$ under our current hypothesis that F_{CO} primarily tracks $\dot{M}_{acc}$. This points to

a simple-minded ("one-dimensional") scenario in which collapse is initiated in dense clumps of finite mass ${M_{env}}^0$ and $\dot{M}_{acc}$ then decreases with time in exact proportion to the remaining envelope mass M_{env}, i.e., $\dot{M}_{acc} = M_{env}/\tau$, where τ is a characteristic time. In this scenario, M_{env}, $\dot{M}_{acc}$, and $M_\star$ have simple exponential dependences with time: $M_{env}(t) = {M_{env}}^0 \times e^{-t/\tau}$, $\dot{M}_{acc}(t) = ({M_{env}}^0/\tau) \times e^{-t/\tau}$, and $M_\star(t) = {M_{env}}^0(1-e^{-t/\tau})$. The characteristic time τ is constrained by the estimated duration T of the self-embedded accretion phase: imposing that 90 % of ${M_{env}}^0$ is accreted during T $\sim 2\times10^5$ yr (e.g., Greene et al. 1994) implies that $\tau \sim 9 \times 10^4$ yr. If we take $f_{ent} = 1$, $\dot{M}_w/\dot{M}_{acc} = 0.1$, and $V_w \sim 150$ km s^{-1} as above, then the outflow momentum flux F_{CO} has the same exponential decrease with time as $\dot{M}_{acc}$ (cf. Eq. (5)). We stress that these time dependences are just meant to be illustrative of a probably much more complicated situation. The specific representations we propose for $\dot{M}_{acc}(t)$, $M_{env}(t)$, and $F_{CO}(t)$ ensure that all these parameters decrease simultaneously with time in a self-consistent way. Qualitatively, one expects such a behavior as a protostellar envelope is dissipated by accretion and eroded by a wind with a progressively wider opening angle.

Assuming that the bolometric luminosity L_{bol} derives entirely from infall/accretion, i.e., $L_{bol}(t) = L_{acc} = G\,\frac{M_\star(t)\dot{M}_{acc}(t)}{R_\star}$ with $R_\star \sim 3$ R$_\odot$ (see, e.g., Stahler 1988), the above scenario leads to indicative evolutionary tracks in the F_{CO}–L_{bol} diagram which we have plotted as (light) dotted curves in Fig. 5 for three initial clump masses (0.3, 0.6, and 1.2 M$_\odot$). Each track reaches a maximum luminosity when half of the initial clump mass has been accreted by the protostar, i.e., when $M_\star = M_{env}$ (with T $\sim 2\times10^5$ yr, this occurs at $t \sim 6\times10^4$ yr). The loci of maximum L_{bol} on the tracks therefore trace the conceptual border line between the Class 0 and Class I evolutionary stages.

This 'toy' model, which ignores complications such as cloud-dependent effects, is clearly oversimplistic. For instance, the tracks of Fig. 5 suggest comparable numbers of 0.3 M$_\odot$ and 1.2 M$_\odot$ objects, which is not realistic even taking into account possible biases in the sample. Nevertheless, the model illustrates the behavior we anticipate for the actual evolutionary tracks. At the earliest (Class 0) stage, the wind is strong due to a high accretion/infall rate, but the luminosity is low because the central mass $M_\star$ is small; since the increase of $M_\star$ dominates, L_{bol} increases with comparatively little variation of F_{CO}, implying a decline of outflow efficiency (see Fig. 5 and Fig. 7). At later times (Class I stage), when $M_\star$ is near its final value and $\dot{M}_{acc}$ has fallen, then both F_{CO} and L_{bol} decrease proportionally to $\dot{M}_{acc}$, so that the outflow efficiency remains nearly constant (as long as $L_{bol} \sim L_{acc}$). This offers a simple explanation for why F_{CO} correlates linearly with L_{bol} for Class I sources and explains the apparent break in outflow efficiency between Class 0 and Class I sources (Fig. 7 and Fig. 5), without any qualitative change in outflow mechanism or entrainment efficiency.

Our purely phenomenological scenario also reproduces the range observed for the various parameters. It accounts for the build up of stars within the duration T $\sim 2\times10^5$ yr generally estimated for the accretion phase. It suggests plausible values of $\dot{M}_{acc}$ for both the beginning and the end of this phase: $\dot{M}_{acc} \sim 10^{-5}$ M$_\odot$yr^{-1} is close to the standard mass infall rate[7] $\dot{M}_{inf} = a^3/G$ expected for the collapse of a cloud core at a temperature $T = 30$ K (Shu 1977), while $\dot{M}_{acc} \sim 2\times10^{-7}$ M$_\odot$yr^{-1} is comparable to the accretion rates derived for the most active T Tauri stars; see Basri & Bertout 1989, Hartmann & Kenyon 1990, Hartigan et al. 1995).

If confirmed, such a time evolution of $\dot{M}_{acc}$ may have important consequences, e.g., for our understanding of the luminosity functions of embedded clusters, since it is at present widely believed (or assumed) that the mass infall rate remains constant during the accretion phase (e.g., Fletcher & Stahler 1994). We also note that the suggested decrease of $\dot{M}_{acc}$ may be the natural result of plausible initial conditions for protostellar collapse. Based on numerical computations, Foster & Chevalier (1993) have indeed found that the collapse of bounded isothermal spheres generally leads to a sharp decline of the mass accretion rate after protostellar core formation (see also Henriksen 1994).

4.3.2. A decline of the entrainment and/or driving engine efficiencies ?

Another way to account for the observed decline of outflow energetics with evolutionary stage is to invoke a decrease with time of the entrainment efficiency f_{ent} or of the outflow driving engine efficiency $(\dot{M}_w/\dot{M}_{acc})\,V_w$ (see Eq. (5)).

The first factor f_{ent} measures the ability with which the entrained ambient gas retrieves the momentum flux of the underlying driving jet/wind at its source. Two basic types of entrainment are believed to occur when a jet interacts with the surrounding quiescent gas: "prompt" entraiment and "steady state" entrainment (De Young 1986). Prompt entrainment refers to momentum transfer through a single working surface, the jet bowshock (see Raga & Cabrit 1993 and Chernin et al. 1994), whereas steady state entrainment corresponds to good sideway coupling between the jet and ambient gas through multiple working surfaces (Raga et al. 1993) or general turbulence (Stahler 1993). While entrainment of the youngest CO outflows is likely to be dominated by the former process, mature outflows are better explained by pure steady state entrainment (Chernin et al. 1994) or by the averaged action of multiple prompt momentum transfers (e.g., Chernin & Masson 1995). Therefore, we may a priori expect f_{ent} to evolve with time due to a change in the basic entrainment process responsible for momentum transfer in the close environment of YSOs. However, our present observations are only weakly sensitive to the extremely high-velocity CO features which characterize prompt entrainment and are observed in the youngest outflows. Our observations mostly probe the low-velocity component present in all CO outflows (see Sect. 3.2) which is likely to be weakly dependent on the exact entrainment process. Therefore, we do not believe that f_{ent} can vary by the

[7] Since massive disks are rare, implying that infalling material cannot accumulate in the disk during most of the protostellar phase (Terebey et al. 1993), the mass infall rate $\dot{M}_{inf}$ in the protostellar envelope is likely to be similar to the disk accretion rate $\dot{M}_{acc}$.

order of magnitude required to explain the correlation seen in Fig. 6.

The second factor $(\dot{M}_w/\dot{M}_{acc})\,V_w$ is directly related to the ejection mechanism and may be considered as a measure of the outflow driving engine efficiency. Both the ratio $\dot{M}_w/\dot{M}_{acc}$ and the jet/wind velocity V_w may vary significantly with time as a YSO accretes more mass (i.e., $M_\star$ increases) and the innermost regions evolve, e.g., with formation and growth of a disk. The wind velocity V_w is unlikely to increase by more than a factor $\lesssim 3$ from Class 0 to Class I sources, since young CO outflows showing extremely high-velocity features have velocities of at least ~ 100 km s^{-1} (e.g., Bachiller & Gómez-González 1992) while the jet velocities measured for active T Tauri stars are ~ 300 km s^{-1} (e.g., Mundt et al. 1987). The variations of the ratio $\dot{M}_w/\dot{M}_{acc}$ may be larger, since theoretical models predict typical values between 0.1 and 0.5 but may account for ratios as low as 10^{-5} (see Sect. 4.3.1). However, all theoretical outflow models involving magnetocentrifugal ejection (Pelletier & Pudritz 1992, Wardle & Königl 1993, Shu et al. 1994) predict the same general behavior: in these models, a decrease of $\dot{M}_w/\dot{M}_{acc}$ is always partly compensated for by an increase of the ejection velocity V_w, so that the factor $(\dot{M}_w/\dot{M}_{acc})\,V_w$ entering Eq. (5) has only small variations. For instance, in the models of Najita & Shu (1994) based on the X-wind mechanism, the factor $(\dot{M}_w/\dot{M}_{acc})\,V_w$ varies only between ~ 50 and ~ 70 km s^{-1} (see their Tables 5 and 6). Likewise, in the magnetized accretion–ejection structures of Ferreira & Pelletier (1995), $(\dot{M}_w/\dot{M}_{acc})\,V_w$ has typical values of ~ 20 km s^{-1} and is proportional to V_w^{-1}; it is therefore unlikely to vary by more than a factor of $\lesssim 3$.

In conclusion, the variations of both f_{ent} and $(\dot{M}_w/\dot{M}_{acc})\,V_w$ are expected to be small during the protostellar phase and are unlikely to account for the order-of-magnitude decrease of F_{CO} observed between the Class 0 and Class I stages.

5. Summary

We have obtained and analyzed a homogeneous set of CO(2–1) data around a large sample of low-luminosity embedded YSOs, including 36 near-IR (Class I) protostars and 9 far-IR/submm (Class 0) protostars. Our main findings may be summarized as follows:

1. Essentially *all* low-mass YSOs show some degree of outflow activity when they are still embedded within a detectable circumstellar envelope. Therefore, outflow phase and infall/accretion phase appear to coincide in low-mass YSOs. This is consistent with the idea that accretion cannot proceed without ejection and that outflows are directly powered by accretion.
2. Class 0 objects lie an order of magnitude above the well-known correlation between outflow momentum flux and bolometric luminosity observed for Class I sources. Inclination effects are unlikely to explain this qualitative difference. Class 0 objects are thus distinguished from Class I sources not only by the strength of their submillimeter continuum emission but also by more powerful CO outflows.
3. On the other hand, outflow momentum flux is found to be roughly proportional to circumstellar envelope mass in the *entire* sample (i.e., including both Class I and Class 0 sources). Since luminosity effects alone cannot account for this tight correlation, we interpret it as an evolutionary effect reflecting a progressive *decline of outflow activity* during the protostellar accretion phase.
4. This positive result we obtain on outflow evolution illustrates the usefulness of M_{env} and M_{env}/L_{bol} as practical age-ordering indicators for embedded YSOs.
5. We suggest that the observed decline of outflow energetics with time results from a decrease of mass accretion/infall rate from $\dot{M}_{acc} \sim 10^{-5}\,M_\odot yr^{-1}$ for the youngest Class 0 protostars to $\dot{M}_{acc} \sim 10^{-7}\,M_\odot yr^{-1}$ for the most evolved Class I sources and most active T Tauri stars.
6. Other factors such as an evolution of ambient gas entrainment by the underlying driving jet and/or a decrease of the jet driving engine efficiency may also play a role, albeit probably less important, in explaining the decline of outflow power with age.

Acknowledgements. We acknowledge the excellent support of the NRAO Tucson, CSO, and IRAM Granada staffs during the observations. We are indebted to Charlie Lada for his contribution in the early phases of the project and for his insightful comments as referee of the paper. We would also like to thank Sergio Molinari, Paolo Saraceno, and Steve Stahler for useful and stimulating discussions. Ph.A. was supported by an NRAO Jansky fellowship at the beginning of this work.

References

André P. 1995, Ap&SS 224, 29
André P., Montmerle T. 1994, ApJ 420, 837 (AM)
André P., Martín-Pintado J., Despois D., Montmerle T. 1990, A&A 236, 180
André P., Ward-Thompson D., Barsony M. 1993, ApJ 406, 122 (AWB)
Bachiller R., Gómez-González J. 1992, A&AR 3, 257
Bachiller R., Cernicharo J., Martín-Pintado J., Tafalla M., Lazareff B. 1990, A&A 231, 174
Bachiller R., André P., Cabrit S. 1991a, A&A 241, L43
Bachiller R., Martín-Pintado J., Planesas P. 1991b, A&A 251, 639
Bally J., Lada C.J. 1983, ApJ 265, 824
Bally J., Lane A.P. 1991, in: Lada C.J., Kylafis N.D. (eds.) The physics of Star Formation and Early Evolution. Kluwer, Dordrecht, p. 471
Basri G., Bertout C. 1989, ApJ 341, 340
Beichman C.A., Myers P.C., Emerson J.P. et al., 1986, ApJ 307, 337
Blandford R.D., Payne D.G. 1982, MNRAS 199, 883
Cabrit S., André P. 1991, ApJ 379, L25
Cabrit S., Bertout C. 1990, ApJ 348, 530
Cabrit S., Bertout C. 1992, A&A 261, 274 (CB)
Cabrit S., Edwards S., Strom S.E., Strom K.M. 1990, ApJ 354, 687
Chernin L.M., Masson C.R. 1995, ApJ 455, 182
Chernin L.M., Masson C.R., Gouveia Dal Pino E.M., Benz W. 1994, ApJ 426, 204
Davidson J.A. 1987, ApJ 315, 602
De Young D.S. 1986, ApJ 307, 62

Edwards S., Ray T., Mundt R. 1993, in: Levy E.H., Lunine J.I. (eds.) Protostars and Planets III. University of Arizona Press, Tucson, p. 567
Feigelson E.D., Nelson P.I. 1985, ApJ 293, 192
Ferreira J., Pelletier G. 1995, A&A 295, 807
Fletcher A.B., Stahler S.W. 1994, ApJ 435, 313
Foster P.N., Chevalier R.A. 1993, ApJ 416, 303
Fukui K., Sugitani K., Takaba H. et al., 1986, ApJ 311, L85
Galli D. 1995, Rev.Mex.A&A Serie de Confer. 1, 179
Goldsmith P.F., Snell R.L., Hemeon-Heyer M., Langer W.D. 1984, ApJ 286, 599
Goldsmith P.F., Langer W.D., Wilson W.W. 1986, ApJ 303, L11
Greene T.P., Wilking B.A., André P., Young E.T., Lada C.J. 1994, ApJ 434, 614
Hartigan P., Edwards S., Ghandour L. 1995, ApJ 452, 736
Hartmann L.W., Kenyon S.J. 1990, ApJ 349, 190
Henriksen R.N. 1994, in: Montmerle T., Lada C.J., Mirabel I.F., Trân Thanh Vân J. (eds.) The Cold Universe. Editions Frontières, Gif-sur-Yvette, p. 241
Heyer M.H., Snell R.L, Goldsmith P.F., Myers P.C. 1987, ApJ 321, 370
Isobe T., Feigelson E.D., Nelson P.I. 1986, ApJ 306, 490
Kenyon S.J., Hartmann L.W., Strom K.M., Strom S.E. 1990, AJ 99, 869
Kenyon S.J., Calvet N., Hartmann L. 1993, ApJ 414, 676
Königl A., Ruden S.P. 1993, in: Levy E.H., Lunine J.I. (eds.) Protostars and Planets III. University of Arizona Press, Tucson, p. 641
Lada C.J. 1985, ARA&A 23,267
Lada C.J. 1987, in: Peimbert M., Jugaku J. (eds.) Star Forming Regions. IAU Symp. 115, Reidel, Dordrecht, p. 1
Lada C.J., Shu F.H. 1990, Sci 248, 564
Ladd E.F., Adams F.C., Casey S. et al., 1991, ApJ 366, 203
Levreault R.M. 1988, ApJ 330, 897
Masson C.R. 1995, Ap&SS 224, 99
Masson C.R., Chernin L.M. 1993, ApJ 414, 230
Masson C.R., Chernin L.M. 1994, PASPC 65, 350
Mauersberger R., Guélin M., Martín-Pintado J. et al. 1989, A&AS 79, 217
Moriarty-Schieven G.H., Snell R.L. 1988, ApJ 332, 364
Moriarty-Schieven G.H., Wannier P.G., Keene J., Tamura M. 1994, ApJ 436, 800
Motte F., André P., Neri R. 1995, in: Siebenmorgen R., Kaufl H.U. (eds.) The Role of Dust in the Formation of Stars. ESO Workshop Series, Springer-Verlag, in press
Mozurkewich D., Schwartz P.R., Smith H.A. 1986, ApJ 311, 371
Mundt R., Brugel E.W., Bührke T. 1987, ApJ 319, 275
Myers P.C., Fuller G.A., Mathieu R.D. et al. 1987, ApJ 319, 340
Myers P.C., Heyer M.H., Snell R.L, Goldsmith P.F. 1988, ApJ 324, 907
Najita J.R., Shu F.H. 1994, ApJ 429, 808
Ossenkopf V., Henning T. 1994, A&A 291, 943
Parker N.D. 1991, MNRAS 251, 63
Parker N.D., Padman R., Scott P.F. 1991, MNRAS 252, 442
Pelletier G., Pudritz R.E. 1992, ApJ 394, 117
Pudritz R.E., Norman C.A. 1986, ApJ 301, 571
Raga A.C., Cabrit S. 1993, A&A 278, 267
Raga A.C., Cantó J., Calvet N., Rodríguez L.F., Torrelles J.M. 1993, A&A 276, 539
Reipurth B., Chini R., Krügel E., Kreysa E., Sievers A. 1993, A&A 273, 221
Rodríguez L.F., Carral P., Ho P.T.P., Moran J.M. 1982, ApJ 247, 461
Saraceno P., André P., Ceccarelli C., Griffin M., Molinari S. 1996, A&A in press
Shu F.H. 1977, ApJ 214, 488
Shu F.H., Adams F.C., Lizano S. 1987, ARA&A 25, 23
Shu F.H., Lizano S., Ruden S.P., Najita J. 1988, ApJ 328, L19
Shu F., Najita J., Ostriker E. et al. 1994, ApJ 429, 781
Stahler S.W. 1988, ApJ 332, 804
Stahler S.W. 1993, in: Livio M., O'Dea C., Burgarella D. (eds.) Astrophysical Jets. Cambridge University Press, New York, p. 183
Terebey S., Shu F.H., Cassen P.C. 1984, ApJ 286, 529
Terebey S., Vogel S.N., Myers P.C. 1989, ApJ 340, 472
Terebey S., Vogel S.N., Myers P.C. 1992, ApJ 390, 181
Terebey S., Chandler C.J., André P. 1993, ApJ 414, 759
Walker C.K., Lada C.J., Young E.T., Maloney P.R., Wilking B.A. 1986, ApJ 309, L47
Ward-Thompson D. 1993, MNRAS 265, 493
Wardle M., Königl A. 1993, ApJ 410, 218
Wilking B.A., Lada C.J., Young E.T. 1989, ApJ 340, 823
Yorke H.W., Bodenheimer P., Laughlin G. 1995, ApJ 443, 199

This article was processed by the author using Springer-Verlag LaTeX A&A style file version 3.